ACS APPLIED MATERIALS & INTERFACES

Research Article

www.acsami.org

Self-Assembled Hierarchical Superstructures from the Benzene-1,3,5-Tricarboxamide Supramolecules for the Fabrication of Remote-Controllable Actuating and Rewritable Films

Yu-Jin Choi,[†] Dae-Yoon Kim,[†] Minwook Park,[†] Won-Jin Yoon,[†] Yumin Lee,[†] Joo-Kyoung Hwang,[†] Yeo-Wan Chiang,[‡] Shiao-Wei Kuo,[‡] Chih-Hao Hsu,[*,§] and Kwang-Un Jeong[*,†]

[†]Polymer Materials Fusion Research Center & Department of Polymer-Nano Science and Technology, Chonbuk National University, Jeonju 561-756, Korea

[‡]Department of Materials Science and Optoelectronic Engineering, National Sun Yat-Sen University, Kaohsiung 804, Taiwan

[§]Department of Polymer Science, The University of Akron, Akron, Ohio 44325-3909, United States

Supporting Information

ABSTRACT: The well-defined hierarchical superstructures constructed by the self-assembly of programmed supramolecules can be organized for the fabrication of remote-controllable actuating and rewritable films. To realize this concept, we newly designed and synthesized a benzene-1,3,5-tricarboxamide (BTA) derivative (abbreviated as BTA-3AZO) containing photoresponsive azobenzene (AZO) mesogens on the periphery of the BTA core. BTA-3AZO was first self-assembled to nanocolumns mainly driven by the intermolecular hydrogen-bonds between BTA cores, and these self-assembled nanocolumns were further self-organized laterally to form the low-ordered hexagonal columnar liquid crystal (LC) phase below the isotropization temperature. Upon cooling, a lamello-columnar crystal phase emerged at room temperature via a highly ordered lamello-columnar LC phase. The three-dimensional (3D) organogel networks consisted of fibrous and lamellar superstructures were fabricated in the BTA-3AZO cyclohexane-methanol solutions. By tuning the wavelength of light, the shape and color of the 3D networked thin films were remote-controlled by the conformational changes of azobenzene moieties in the BTA-3AZO. The demonstrations of remote-controllable 3D actuating and rewritable films with the self-assembled hierarchical BTA-3AZO thin films can be stepping stones for the advanced flexible optoelectronic devices.

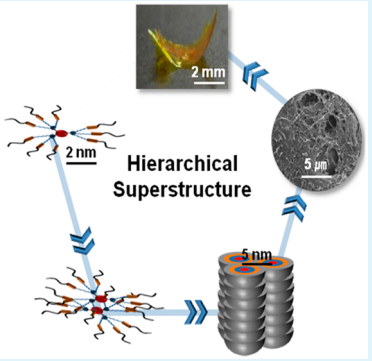

KEYWORDS: *supramolecule, self-assembly, remote-control, reversible actuating, rewritable film*

INTRODUCTION

The development of supramolecular chemistry provides a platform for the design and synthesis of multifunctional molecules which can evolve into the self-assembled superstructures with the targeted physical properties.[1] On the basis of the programmed physical interactions, such as hydrogen-bonding (H-bonds), $\pi-\pi$ stacking, and van der Waals force, the hierarchical superstructures can be precisely controlled with and without the support of external forces, such as surface anchoring force, temperature, and concentration gradients, and electrical and magnetic fields.[2−4] Among these secondary interactions, the directional H-bonds can be a very useful physical bond for the fabrication of the well-defined hierarchical superstructures.[5]

Because the self-assembly of supramolecules depends not only on the chemical structures but also on various external stimuli, such as light, temperature, pH, and electric and magnetic fields, the reversible behaviors of supramolecular structures responding to the external stimuli have attracted considerable attention for their practical applications including reversible actuating and rewritable films.[6−11] Among many candidates, the photoresponsive azobenzene-based supramolecules can be effectively applied for the remote-controllable systems.[12−14] Even though the self-assembly is a very effective approach to control the molecular packing structures with tunable properties, the supramolecule-based actuating materials are still not comparable with polymeric systems in terms of processability and stability. As a result, many efforts have been devoted for the development of novel supramolecules and their hierarchical superstructures with enhanced physical performances and stabilities.[15,16] The self-assembled liquid crystalline (LC) materials with the reasonable high mobility and processability can be potential materials to overcome the limitations of traditional supramolecules.[17,18] However, to precisely modulate their physical properties, we must understand the mechanism of self-assembly and the constructed superstructures on the different length scales.

Received: March 19, 2016
Accepted: March 29, 2016
Published: March 29, 2016

DOI: 10.1021/acsami.6b03364
ACS Appl. Mater. Interfaces 2016, 8, 9490−9498

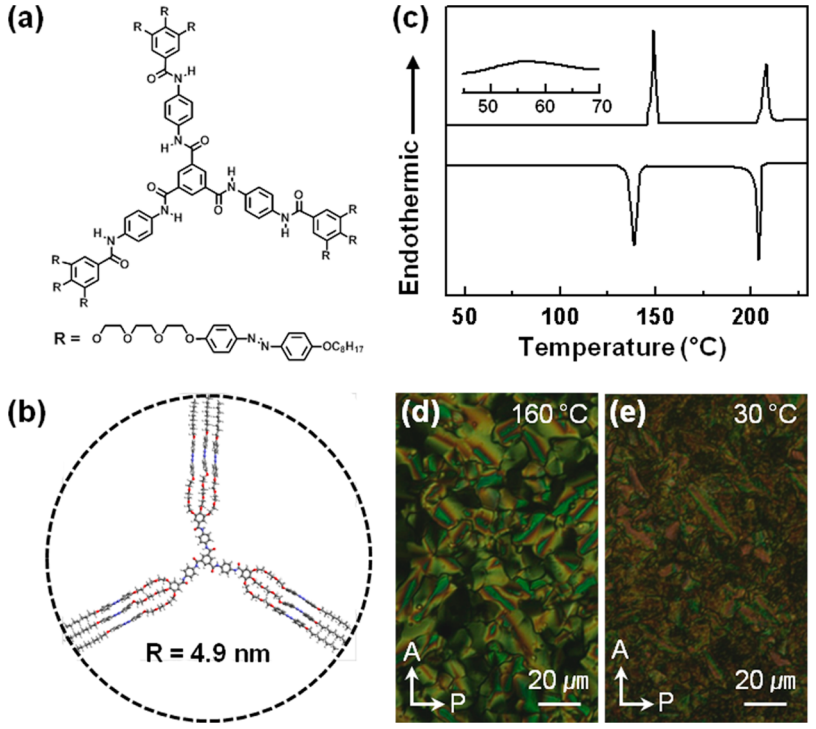

Figure 1. (a) Chemical structure of BTA-3AZO and (b) its energy minimized molecular geometry. (c) DSC thermograms of BTA-3AZO at 2.5 °C/min. POM images of BTA-3AZO at (d) 160 and (e) 30 °C.

From this perspective, we newly design and synthesize a benzene-1,3,5-tricarboxamide (BTA) derivative containing photoresponsive azobenzene mesogens (AZO), as shown in Figure 1a. The programmed supramolecule is abbreviated as BTA-3AZO. Benzene-1,3,5-tricarboxamide molecule is consisted of a benzene core and three amides tethered to the benzene ring at the 1,3,5-positions via the carbonyl linkage, yielding the BTA core. The BTA derivative has a 3-fold rotational symmetry (C_3). By further tethering functional groups to the amides, BTA derivatives can be the building blocks of the well-defined superstructures.[19−21] For the precise control of hierarchical superstructures on the multiple length scales, the molecular design of BTA-3AZO is based on the following three considerations: (1) the photoirradiation can lead to the *trans*-to-*cis* isomerization and the *cis*-to-*trans* isomerization of the azobenzene moieties, resulting in the molecular conformational changes; (2) the molecular nanophase separations between hydrophilic and hydrophobic moieties in the BTA-3AZO are critical for the construction of well-defined hierarchical superstructures; and (3) the incorporation of directional intermolecular H-bonds between amide groups can enhance the processability of gel formations and the mechanical stabilities. With the combined techniques of differential scanning calorimetry (DSC), cross-polarized optical microscope (POM) and Fourier transform infrared spectroscopy (FT IR), the phase evolutions of BTA-3AZO are investigated. The molecular packing structures are identified by wide-angle X-ray diffraction (WAXD) and small-angle X-ray scattering (SAXS) of oriented samples, and the proposed packing models are further confirmed by the computer simulation on the reciprocal and real spaces. To demonstrate the BTA-3AZO for remote-controllable 3D actuating and rewritable films, the organogel 3D networks consisted of fibrous and lamellar superstructures are fabricated in the BTA-3AZO cyclohexane-methanol solutions. The shape and color of the self-assembled thin films are remote-controlled by tuning the wavelength of light.

RESULTS AND DISCUSSION

Programmed Benzene-1,3,5-Tricarboxamide Supramolecule. The BTA-3AZO is prepared according to the synthetic routes, as shown in Scheme S1. Compound 1 with three azobenzene groups is synthesized via the procedures in our previous publication.[22] Compound 1 is reacted with *p*-phenylenediamine in methylene chloride (MC) and tetrahydrofuran (THF) (v/v = 4:1) in the presence of *N,N′*-diisopropylcarbodiimide (DIPC) and 4-(dimethylamino) pyridinium 4-toluenesulfonate (DPTS) at room temperature. The targeted BTA-3AZO compound is prepared by a coupling reaction with the benzene-1,3,5-tricarbonyl chloride and compound 2 in THF. The synthetic details and characterization data are summarized in the Supporting Information. Chemical structures of BTA-3AZO are confirmed by ^{1}H NMR (Figures S1 and S2), ^{13}C NMR (Figure S3), MALDI-ToF mass spectrometry (Figure S4), and elemental analysis (Table S1). The calculated molecular dimensions and energy minimized geometry of BTA-3AZO is estimated using Cerius^2 simulation software from Accelrys (version 4.6). The calculated radius of BTA-3AZO is 4.9 nm (Figure 1b).

Phase Transitions and Structure Evolution. The phase transition behaviors of BTA-3AZO are investigated by DSC combined with POM. Figure 1c shows DSC thermograms of BTA-3AZO upon cooling and subsequent heating at 2.5 °C/min. A set of DSC thermograms at various scanning rates is additionally provided in Figure S5. In Figure 1c, two exothermic thermal transitions are detected during the cooling process. The high-temperature transition appears at 204.1 °C with a heat of transition (35 kJ/mol), which is independent of the cooling rate. Although the width of the high-temperature

DOI: 10.1021/acsami.6b03364
ACS Appl. Mater. Interfaces 2016, 8, 9490−9498

transition is broadened with increasing the cooling rate, the rate-independent of exothermic transition and its corresponding heat clearly indicate that the first-order transition takes place close to the thermodynamic equilibrium. On the other hand, the onset temperatures of the low-temperature exothermic transition shift to lower temperatures as the cooling rate increased (Figure S5b). At the cooling rate of 2.5 °C/min, the onset temperature of the low-temperature exothermic transition is 141.4 °C with 43.3 kJ/mol. However, the onset temperature and the heat of transition at 20 °C/min are 137.6 °C and 33.3 kJ/mol, respectively. Upon heating, two sharp endothermic peaks are observed at 204.9 °C (43.4 kJ/mol) and 146.8 °C (27.3 kJ/mol) for all the heating rates. Additionally, a relatively broad peak at 60 °C is detected, which is often observed in the supramolecules with alkyl tails, as shown in the inset of Figure 1c.

To evaluate the formation of ordered structures, POM experiments are conducted by cooling from the isotropic (I) state to room temperature at 2.5 °C/min, as shown in Figure S6. The optical images show the fan-shaped focal conic texture at the 160 °C (Figure 1d), which is often observed in a typical columnar LC phase.[23,24] Further decreasing the temperature to room temperature results in the solidification with birefringent defects (Figure 1e) which are mainly generated due to the anisotropic volume shrinkages. The POM results combined with those of DSC reveal that three ordered phases are formed below the isotropization temperature (T_i = 206 °C): a low-ordered LC phase, a highly ordered LC (K_{LC}) phase, and a crystal (K_{Cr}) phase.

To understand the molecular packing structures, BTA-3AZO in the bulk state is investigated by 1D WAXD and SAXS experiments at different temperatures. Figure 2a shows 1D WAXD powder patterns obtained during cooling at 2.5 °C/min. In this figure, structures on two different length scales can be identified. The low-angle region between 1.5 and 9° provides the nanometer scale information, such as the periodicity of electron fluctuations between the phase-separated aromatic cores and tails. The subnanometer scale information can be obtained at high-angle region between 9 and 35°. As shown in Figure 2a, the I phase is confirmed at 210 °C by the observation of two amorphous halos located at 2θ angle of 2.16° (d spacing = 4.09 nm) and 19.91° (d spacing = 0.45 nm), respectively. In the 1D WAXD pattern recorded at 160 °C, the center location of the high-angle scattering halo slightly shifts to a lower 2θ angle from 19.91 to 19.84° with the decreased full width at half-maximum (fwhm). Additionally, 1D SAXS patterns of the different temperature regions exhibit sharp scattering peaks and higher order peaks (Figure 3). The observation of diffractions with the q-value ratio of $1:\sqrt{3}:\sqrt{7}$ (d spacing = 5.42, 3.12, and 2.04 nm) in Figure 3c indicates a hexagonal packing of the self-assembled nanocolumns (stacking of cores via H-bonds) below T_i = 206 °C.[25−27] When the temperature reaches to 100 °C (below the LC phase, Figure 3b), the newly emerged set of diffractions with the q-value ratio of 1:2:3 (d spacing =7.18, 3.51, and 2.36 nm) superimposes on another set of diffractions with the d spacings of 4.32 and 3.25 nm. The origins of two sets of diffractions need to be resolved by further 2D SAXS experiments.[28,29] The shifting and narrowing of the high-angle scattering halo during cooling indicate the increase of the correlation length and the closer molecular lateral packing. Upon further cooling to 25 °C, the 1D SAXS peak with the d spacing = 7.18 nm slightly shifts to the d spacing = 7.28 nm in the 1D SAXS patterns (Figure 3a),

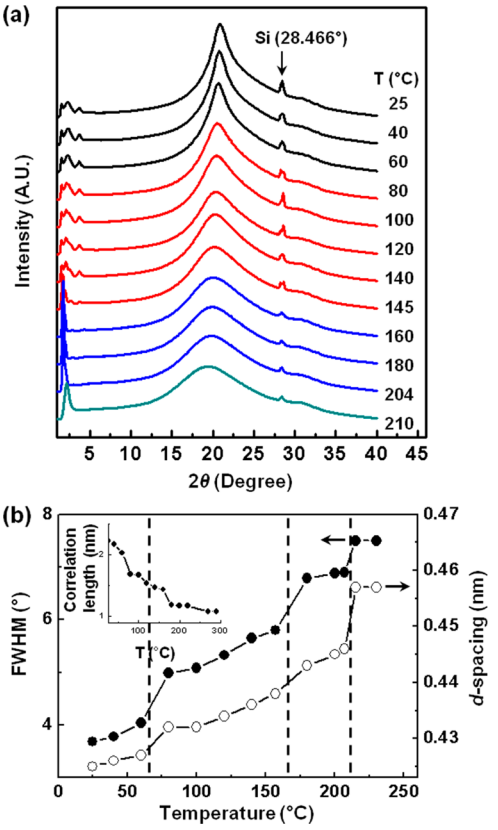

Figure 2. (a) 1D WAXD powder patterns of BTA-3AZO at different temperatures during cooling at 2.5 °C/min. (b) The relationship of the d spacing of scattering halo (2θ = 19.9°) and the corresponding correlation length of BTA-3AZO. (b, inset) Correlation lengths; here, silicon power (2θ = 28.466°) is used as a calibration material.

indicating the formation of highly ordered phase structures. On the basis of experimental results of 1D WAXD and SAXS, it is concluded that the LC phase is a traditional hexagonal columnar (Φ_{LC}) phase and the molecular packing structure between K_{LC} phase and K_{Cr} phase does not significantly change during the phase transition. The K_{Cr} phase should be mainly originated from the alkyl tails, which are closely packed in the 3D long-range ordered crystal.

The structural changes of BTA-3AZO can also be demonstrated by the d spacing changes and the alteration in fwhm of high 2θ angle scattering halo with respect to temperatures between 25 and 220 °C (Figure 2b). The abrupt changes of fwhm upon heating and cooling (Figure 2b) match the transition temperatures (vertical dashed lines) observed on the DSC cooling traces very well. The corresponding correlation lengths of the high 2θ angle scattering halo are also estimated by Scherrer equation and shown in the inset of Figure 2b.[30−32]

Molecular Origins of the Phase Transformations. To identify the possible molecular origins of structural evolution, we obtained FT IR spectra at different temperatures and compared with the corresponding DSC results. With careful examination of wavenumber, absorption intensity, and shape at different temperatures, the conformational and molecular interactions of BTA-3AZO in phases and during phase transitions can be understood. Figure 4 represents a set of FT IR spectra of BTA-3AZO, which is prepared by heating at 2.5 °C/min from the room temperature to T_i = 206 °C. The

DOI: 10.1021/acsami.6b03364
ACS Appl. Mater. Interfaces 2016, 8, 9490−9498

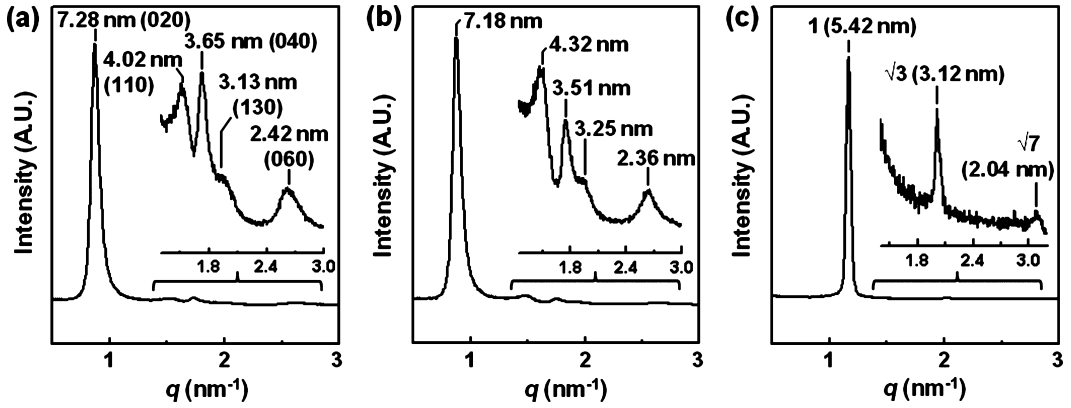

Figure 3. 1D SAXS patterns of BTA-3AZO at (a) 25, (b) 100, and (c) 160 °C, respectively.

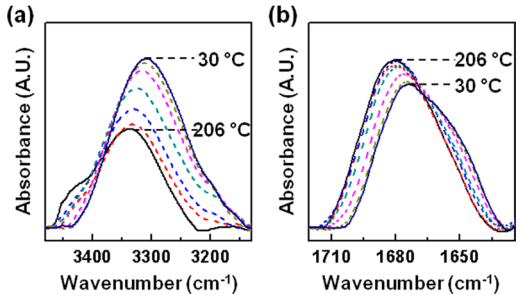

Figure 4. FT IR spectra of BTA-3AZO during cooling at 2.5 °C/min: (a) between 3480 and 3130 cm^{-1} and (b) between 1720 and 1620 cm^{-1}.

overall FT IR spectra of BTA-3AZO during cooling from T_i = 206 to 30 °C at 2.5 °C/min are also provided in Figure S7. The H-bonds between the N−H group and the C═O of amide unit in BTA-3AZO strongly influence the formation of ordered structures. It is well-known that the H-bonds are sensitive to N−H stretching vibration band (3286 and 3056 cm^{-1}) and amide I mode (1661 cm^{-1}).[33−35] As increasing the temperature from the K_{Cr} phase at 2.5 °C/min, the absorption intensity and area of H-bonded N−H band are decreased. Meanwhile, the intensity of free N−H band is intensively increased with a gradual shift of maximum intensity from 3306 to 3338 cm^{-1} as shown in Figure 4a. The amount of H-bonded C═O band of the amide I mode is decreased along with increasing the intensity and area of the band for H-bonded C═O band in disordered domains as shown in Figure 4b. As the temperature is further reached to T_i = 206 °C, the free N−H group band slightly appeared at 3448 cm^{-1} and another absorption band at 1680 cm^{-1}, which corresponds to the free C═O, appears at the same time. Although these H-bonds gradually become weaker upon increasing the temperature, they still remain at the whole temperature range until reaching T_i = 206 °C.

Identification of Phase Structures of BTA-3AZO. To precisely determine the structural symmetry and lattice parameters, 2D WAXD experiments are conducted for oriented samples. Macroscopically aligned BTA-3AZO samples are prepared by the mechanical extrusion at 160 °C. To obtain the K_{Cr} phase structures, the oriented sample is further annealed by cooling from 130 °C to room temperature at 2.5 °C/min. A series of 2D WAXD patterns for the oriented BTA-3AZO crystals are obtained with the incident X-ray beam parallel to the extruded direction (ED, *z* axis), the *y* axis and the *x* axis, respectively (Figure 5a).

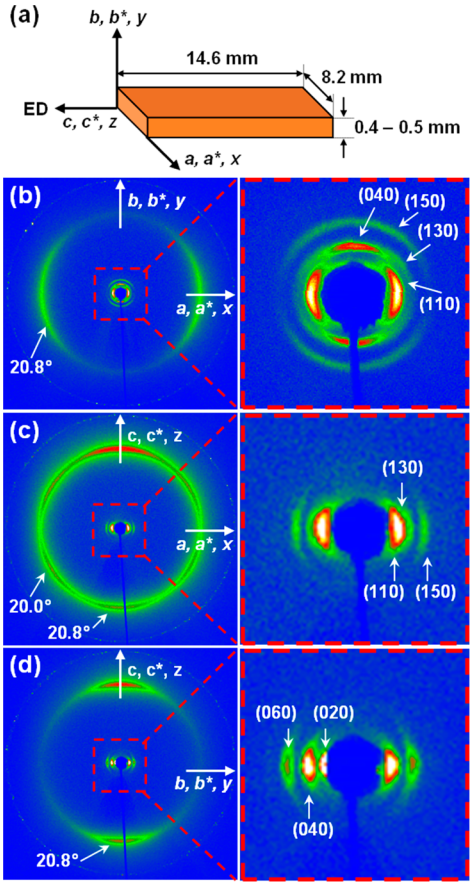

Figure 5. (a) Schematic illustration of the mechanically sheared BTA-3AZO specimen. 2D WAXD patterns of lamello-columnar crystal phase (K_{Cr}) of BTA-3AZO at 25 °C in the (b) [001], (c) [010], and (d) [100] zones. Here, ED means the extruded direction, and *xyz*, *abc*, and *a*b*c** are Cartesian coordinates representing specimen and unit cell geometries in real and reciprocal spaces, respectively.

When the X-ray beam is irradiated parallel to the ED (*z* axis), the 2D WAXD pattern of [001] zone is obtained as shown in Figure 5b. A pair of diffraction arcs at 20.8° (*d* spacing = 0.44 nm) related to intermolecular interactions between the alkyl tails of BTA-3AZO molecules is detected on the equator, indicating the long axis of the alkyl tails oriented parallel to the *b* axis. Figure 6a shows the corresponding 2D SAXS pattern of [001] zone (Figure 5b) at the low angle region. The diffraction arcs can be indexed based on an orthogonal 2D lattice, as

DOI: 10.1021/acsami.6b03364
ACS Appl. Mater. Interfaces 2016, 8, 9490−9498

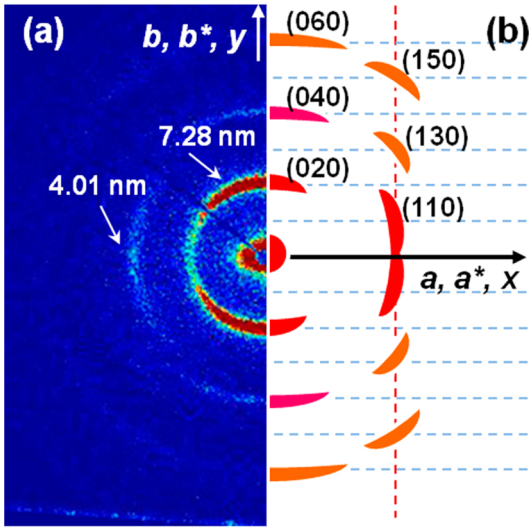

Figure 6. (a) The [001] zone of 2D SAXS pattern for K_{Cr} phase of BTA-3AZO at 25 °C and (b) the corresponding schematic illustrations of indexes.

illustrated in Figure 6b. The strong diffractions (2θ = 20.8°) on the meridian of Figure 5c,d indicate that the BTA cores stack along the extruded direction to form columns. In the Figure 5c, a pseudohexagonal pattern in superimposed with the diffraction of BTA core stacking. The diffraction arcs located at 2θ = 20.8 and 20.0° with an included angle of 58° are attributed to the packing of AZO mesogens (Figure 7). The sub-lattice consisting of AZO mesogens and alkyl tails in the hierarchical structure is then determined as a 2D orthogonal lattice with a' = 0.52 nm and b' = 0.85 nm (Figure 7a), and the details of crystallographic data are also summarized in Table S2. The corresponding simulated WAXD pattern (Figure 7b) confirms the pseudohexagonal feature. Based on the SAXD pattern (Figure 6) and low angle regions of WAXD patterns (Figure 5), the supramolecular structure consists of the columns of BTA cores (Figure 8a) can be constructed with lattice parameters of a = 4.17 nm, b = 14.56 nm, c = 0.43 nm, and $\alpha = \beta = \gamma = 90°$ (Figure 8b).[36] With four molecules in a lattice, the calculated density is 1.25 g/cm^3, which matches the experimentally measured density of 1.25 g/cm^3. On the basis of the molecular dimension and energy minimization results of BTA-3AZO (Figure S8a), the dashed triangles outline the contours of the top-view of BTA-3AZO columns. Due to the flexibility of the linkers and the assemby of AZO mesogens and alkyl tails, the BTA-3AZO columns do not adopt a hexagonal packing. Instead, the BTA-3AZO columns form a lamello-columnar crystal phase with the lamellar periodicity of alternating BTA-layer and AZO layer along the b axis. The corresponding simulated X-ray pattern (Figure 8b) matches the SAXD pattern along [001] zone (Figure 6), confirming the determined supramolecular hierarchical structure. Projections of molecular packing in the lamello-columnar structure along a axis and b axis are represented in Figure S8b,c. Table S3 lists the experimentally observed and the calculated d spacings based on the orthorhombic lattice.

The molecular packing structure of the low-ordered LC phase (Φ_{LC}) is also studied by the 2D WAXD patterns, with the incident X-ray beam directions parallel to the x axis (Figure 9a) of mechanically sheared sample. The evolution of SAXS patterns with X-ray parallel to the three axes is summarized in

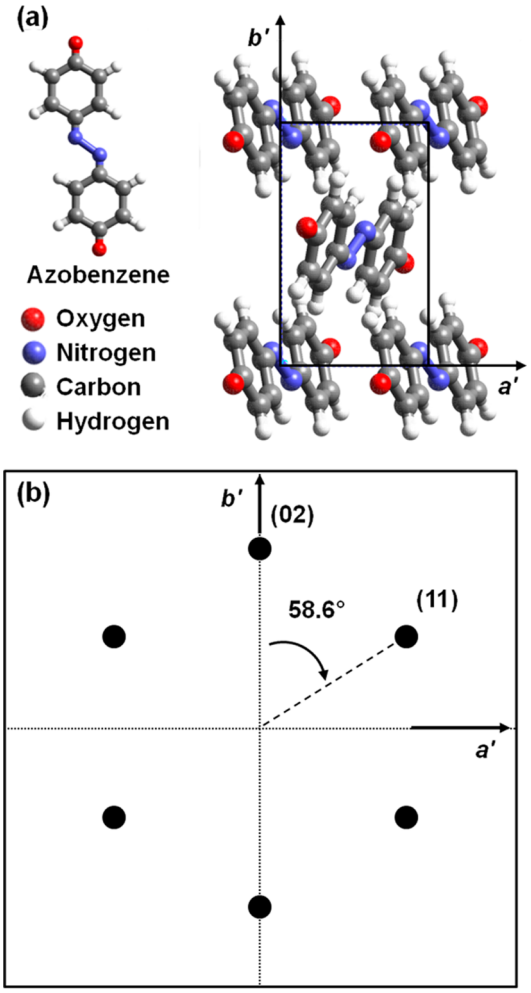

Figure 7. (a) Chemical structure of azobenezene and schematic illustration of the 2D orthogonal sub-lattice of azobenzene in the BTA-3AZO hierarchical structure. (b) Computer-simulated 2D WAXD pattern on the [010] zone (the wide-angle region of Figure 5c) in the K_{Cr} phase.

Figure S9. Above the dissociation temperature of AZO packing, BTA-3AZO molecules undergo a phase transition from the K_{LC} phase to the Φ_{LC} phase between 160 and 205 °C (Figure 2a). The scattering rings in the low angle region of Figure S9a″ indicate the ab-plane of the hexagonal lattice is randomly or inplane oriented along the extrusion direction, and the diffused halo at the 2θ = 20.8° (d spacing = 0.44 nm) is attributed to the disordered alkyl chains. The strong reflections on the meridian (Figure 9b) indicate the existence of stacking of cores, and the diffractions in the low angle region confirm the lateral packing of hexagonally organized columns of stacking cores. Similar to the 2D WAXD of K_{Cr} phase, the 2D WAXD of the Φ_{LC} phase is maintained by intermolecular interactions between the cores. Inferring from the FT IR result that H-bonds still existed below the isotropic temperature at 180 °C, H-bonds between benzene-1,3,5-tricarboxamides are preserved for the self-assembled columns. This can be evidenced by the SAXS pattern of BTA-3AZO in the Figure 3c. The BTA cores construct the column, and then the columns are laterally close-packed into the hexagonal columnar structure as described in Figure 9b. By assigning the diffraction at 2θ = 20.8° as the (001) plane, the phase at 160 °C can be identified as the low-ordered hexagonal columnar LC phase with the hexagonal

DOI: 10.1021/acsami.6b03364
ACS Appl. Mater. Interfaces 2016, 8, 9490−9498

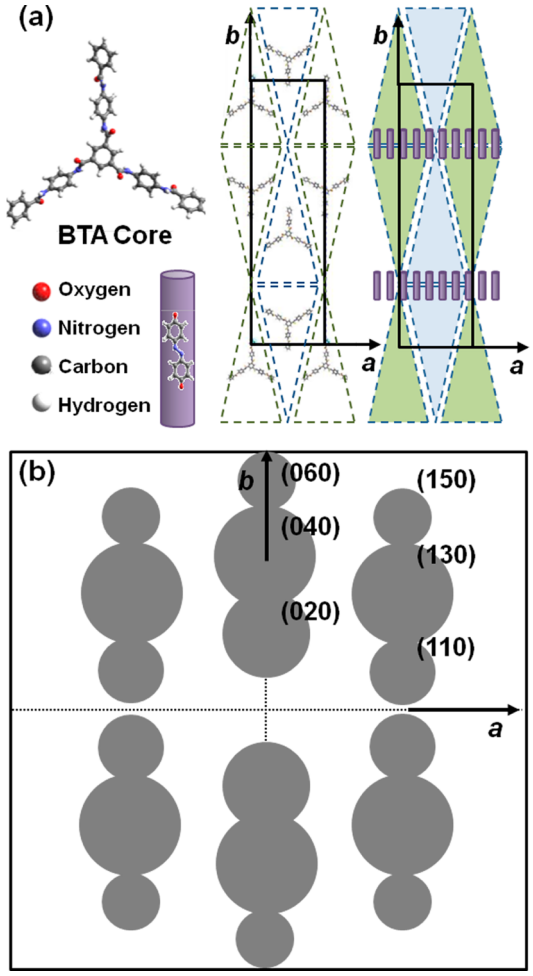

Figure 8. (a) Calculated geometric dimensions of the BTA-3AZO and computer-simulated molecular packing in the *ab* plane of lattice and schematic illustration in the real space, and (b) computer simulated 2D WAXD pattern on the [001] zone (the small-angle region of Figure 5b, and Figure 6) in K_{Cr} phase.

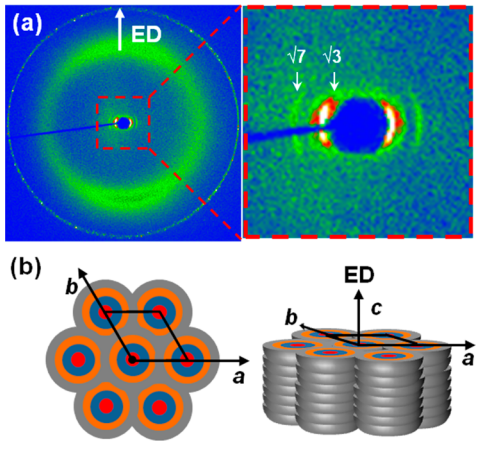

Figure 9. (a) 2D WAXD patterns of hexagonal columnar LC phase (Φ_{LC}) of BTA-3AZO at 160 °C with the incident X-ray beam parallel to the *x* direction of the mechanically extruded specimen. (b) Molecular packing models of the BTA-3AZO.

lattice parameters of $a = b = 5.42$ nm, $c = 0.43$ nm, and $\gamma = 120°$.[37]

Sol–Gel Transitions of Photo-Responsive Organogels. The six H-bondable amide units in the BTA core play a key role to form the macroscopic organogels. Organogels are various 3D aggregates with micro- and nanoscale diameters in the organic solvents. Reversible gelation processes allow us to fabricate exquisite nanostructures.[38−40] Gelation of BTA-3AZO in various organic solvents is summarized in Table S4. Stable transparent organogels are formed when a few drops of methanol are introduced into the 1 wt % BTA-3AZO cyclohexane solution without any precipitaion and crystallization. The macroscopic gelation indicates the formation of elongated fibers and ribbons, which are confirmed by SEM observation as shown in Figure S10. The 1D WAXD pattern of organogel films corresponds to the molecular packing structure of powder pattern in Figure 2a. The organogels composed of the fiberous and lamellar superstructures result in a stable and ductile 3D networked film at room temperature.

The photographs of sol–gel transition process are shown in Figure 10a. Upon UV irradiation (365 nm), the stable organogels are gradually collapsed and turned into the sol state within 10 min, resulting in the photoinduced H-bonds breaking by the *trans*-to-*cis* isomerization (the middle sample in Figure 10a). Subsequently, the organogel is regenerated by the irradiation of visible irradiation (450 nm), as shown in the right side of Figure 10a. The *trans* isomers stabilized by intermolecular interactions can preserve the 3D self-assembled superstructures. The sol–gel phase transitions are reversible without any decompositions of materials.

To understand the photochemical behavior of azobenzene-tapered mesogens (Figure 10 b) in the chloroform solutions (1.25×10^{-3} mg/mL), we obtained UV–vis light absorption spectra, as shown in Figure 10c,d.[41−43] As azobenzene groups transform from the *trans* to the *cis* isomers, the higher polarity and the lower solubility than the *trans* isomers give rise to alter the self-assembled structure as shown in Figure 10c.[44] Upon subsequently exposing the visible light, the *trans* isomer is recovered in the Figure 10d.

Remote-Controllable 3D Actuating and Rewritable Films. To demonstrate writing and erasing a specific pattern[45] on the BTA-3AZO film (Figure 11), we prepared the thin films of self-assembled BTA-3AZO by drop-casting a BTA-3AZO solution (chloroform) on a glass plate. A photomask is introduced between the UV light source and the BTA-3AZO film. The micropatterned BTA-3AZO film is shown in Figure 11a. The UV irradiated area turns bright and the blocked area by the photomask is remained as a dark state. When the temperature of BTA-3AZO film on the glass substrate is increased to 210 °C (above T_i = 206 °C), the BTA-3AZO film turns a bright yellow and the patterns are completely erased for next new patterning processes (Figure 11b).

Photoresponsive LC polymers have been reported as 3D actuators by irradiating the polarized UV lights. Ikeda's group demonstrated that the photoenergy of exposed UV light is converted into the mechanical deformation.[46−49] Note that the effective bending deformation in the polymer systems is partially due to the chemical cross-links, whereas we adopt the self-assembly process of supramolecules for the bending deformation without any polymer network. The self-assembly process for hierarchical thin films can overcome the limitations of processability and stability in the supramolecular systems. Because the BTA-3AZO molecules exhibiting the LC behaviors can form the hierarchical 3D superstructures, thin films and free-standing films are fabricated by the programmed self-

DOI: 10.1021/acsami.6b03364
ACS Appl. Mater. Interfaces 2016, 8, 9490−9498

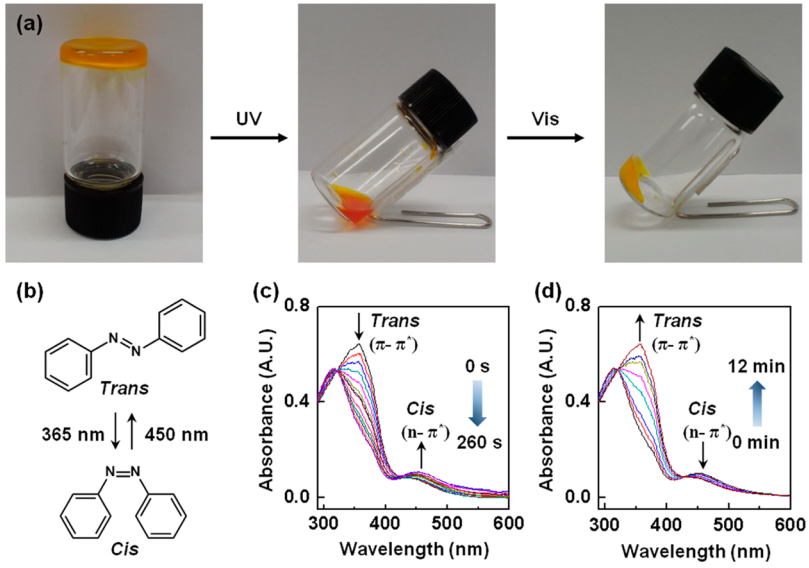

Figure 10. Reversible gel−sol phase transitions of (a) organogel in 1 wt % cylohexane with MeOH upon the UV−vis irradiations. (b) Conformational changes of azobenzene molecule. Photoisomerization of BTA-3AZO (1.25×10^{-3} mg/mL in $CHCl_3$); (c) the *trans* to *cis* isomerization upon the UV irradiation at 365 nm and (d) the reversible *cis*-to-*trans* isomerization upon the vis irradiation at 450 nm.

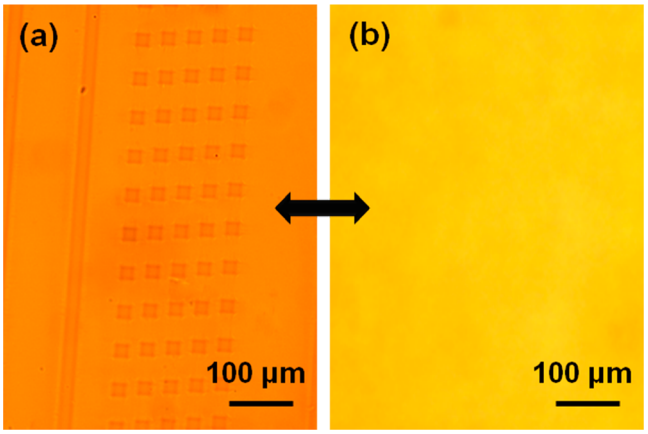

Figure 11. Writing the micropatterns on the BTA-3AZO thin-film at 25 °C (a) after exposing the UV light through the patterned photomask and (b) after erasing them by heating up to 210 °C.

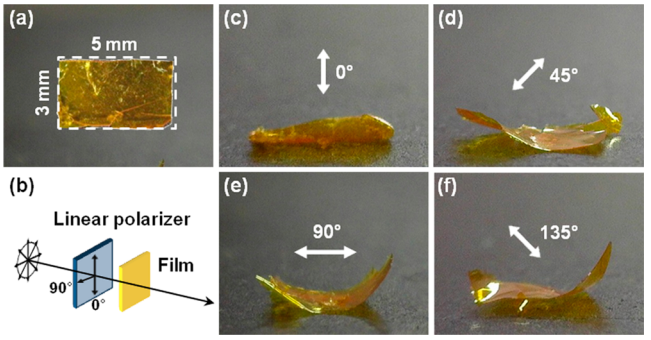

Figure 12. (a) Free-standing BTA-3AZO film and (b) a schematic illustration of 3D actuating experiment with linear polarized UV lights. Photographic images of bending deformations: the precise control of bending directions by exposing the linear polarized light with different angles at (c) 0, (d) 45, (e) 90, and (f) 135°.

assembly process. The free-standing BTA-3AZO films are exquisitely prepared by casting a BTA-3AZO solution (0.1 g/mL in chloroform) on a poly(vinyl alcohol) (PVA) coated glass substrate. As the PVA is dissolved in water, the free-standing films are separated from the glass substrate. A piece of BTA-3AZO film is cut off with dimensions of 5 mm × 3 mm × 15 μm. The center picture of Figure 12a shows the flat film prior to the UV irradiation. When the polarized UV light at 365 nm is exposed (Figure 12b), the macroscopic film deformation is generated toward the irradiating direction within 5 min. The bent films are reversibly transformed to the initial flat film by exposing the vis light. It takes a long time over several hours. Bending directions can be controlled by varying the polarized light axis from 0 to 135°, as shown in Figure 12.

CONCLUSIONS

A benzene-1,3,5-tricarboxamide (BTA) supramolecular building block (BTA-3AZO) was newly designed and successfully synthesized for the construction of the well-defined hierarchical superstructures on the different length scales via the self-assembly processes. To remote-control the physical properties of hierarchical BTA-3AZO superstructures, photoresponsive azobenzene (AZO) mesogens were specifically introduced on the periphery of the BTA core. From the scattering, microscopic and spectroscopic results combined with thermal analyses, it was realized that the programmed BTA-3AZO formed the low-ordered hexagonal columnar LC (Φ_{LC}) phase, the highly ordered lamello-columnar LC (K_{LC}) phase and the lamello-columnar crystal (K_{Cr}) phase. Below the isotropization temperature (T_i = 206 °C), the programmed BTA-3AZO supramolecules first formed the self-assembled nanocolumns mainly driven by the intermolecular hydrogen-bonds between BTA cores with the support of nanophase separation between the hydrophilic core and hydrophobic alkyl tails. The self-assembled nanocolumns were further self-organized laterally to form the Φ_{LC} phase at higher temperatures. Alkyl tails were disordered in the K_{LC} phase, while the ordered alkyl tails did participate for the construction of well-ordered K_{Cr} phase. From the scattering results combined with computer simulations, it was found that the K_{Cr} phase was formed with the lattice parameters of a = 4.17 nm, b = 14.56 nm, c = 0.43

DOI: 10.1021/acsami.6b03364
ACS Appl. Mater. Interfaces 2016, 8, 9490−9498

nm, and $\alpha = \beta = \gamma = 90°$. The organogel 3D networks consisting of fibrous and lamellar superstructures were fabricated in the BTA-3AZO cyclohexane−methanol solutions. Because the shape and color of the robust hierarchical BTA-3AZO thin films were remote-controlled by the conformational changes of azobenzene moieties in the BTA-3AZO, we successfully demonstrated the remote-controllable 3D actuating and rewritable films by tuning the wavelength of light.

EXPERIMENTAL SECTION

Material Preparations. *N-(4-Aminophenyl)-3,4,5-tris[2-(2-{2-(4-((4-(octyloxy)phenyl)diazenyl)phenoxy)ethoxy}ethoxy)ethoxy]-benzamide (i).* To a solution of compound 1 (0.57 g, 0.98 mmol) in MC/THF (40 mL/10 mL) were added DIPC (0.62 g, 4.93 mmol) and DPTS (0.5 g, 0.49 mmol). After the solution was stirred at room temperature for 20 min, *p*-phenylenediamine (1.07 g, 9.85 mmol) was added as a solid, and the suspension was sonicated in an ultrasound bath until the mixture solution was homogeneous. The resulting solution was stirred under nitrogen for 24 h at room temperature. At the end of this period, it was poured into 100 mL of distilled water and extracted with MC. The organic layer was thoroughly dried by anhydrous $MgSO_4$ and solvents were removed. The residue was purified by column chromatography with silica gel using MC:THF = 3:1 after chromatography, products were reprecipitated out from $CHCl_3$ and MeOH and dried under vacuum to afford compound 1 as a yellow powder (Yield: 70%). ^{1}H NMR ($CDCl_3$): δ = 0.89 (t: 9H), 1.23−1.51 (m: 30H), 1.80 (m: 6H), 3.60 (s: 2H), 3.76 (m: 12H), 3.88 (m: 12H) 4.02 (t: 6H), 4.18 (m: 12H), 6.65 (d: 2H), 6.75 (d: 2H), 6.99 (q: 12H), 7.14 (s: 1H), 7.36 (d: 2H), 7.83 (q: 12H).

BTA-3AZO (ii). A mixture of 9 (0.49 g, 0.31 mmol), benzene-1,3,5-tricarbonyl chloride (0.02 g 0.08 mmol) and pyridine (0.05 g, 0.62 mmol) in dried THF (10 mL) were added under nitrogen. The reaction mixture was stirred for 24 h at room temperature. The precipitates were removed by filtration. After evaporation of the solvent, the crude product was purified by column chromatography on silica gel using $CHCl_3$/MeOH = 10:1 (v/v). The resulting product was yellow solid (Yield: 45%) 1H NMR ($CDCl_3$, DMSO-d_6): δ = 0.6 (t: 27H), 1.01−1.17 (m: 90H), 1.50 (m: 12H), 3.46 (m: 36H), 3.58 (m: 36H), 3.72 (m: 18H) 3.88 (t: 36H), 6.69 (m: 36H), 7.04 (m: 6H), 7.53 (m: 48H), 8.52 (s: 3H), 9.40 (s: 3H), 9.72 (s: 3H). ^{13}C NMR ($CDCl_3$, DMSO-d_6): δ = 164.7, 160.5, 159.9, 151.56, 146.23, 145.96, 138.51, 123.58, 123.52, 120.47, 120.27, 114.07, 113.96, 107.0, 70.08, 70.00, 68.99, 68.83, 68.23, 67.59, 67.01, 31.01, 28.56, 28.42, 25.24, 21.86, 13.41.

ASSOCIATED CONTENT

Supporting Information

The Supporting Information is available free of charge on the ACS Publications website at DOI: 10.1021/acsami.6b03364.

Experimental method. Synthetic routes, ^{1}H NMR, ^{13}C NMR, MALDI-ToF MS, EA, DSC, POM images, FT IR, molecular models, and computer simulated molecular packing structure; tables of experimentally observed and the calculated *d* spacings for the *sub* lattice and K_{Cr} phase. 2D SAXS patterns, table of gelation properties, and SEM images. (PDF)

AUTHOR INFORMATION

Corresponding Authors

*E-mail: kujeong@jbnu.ac.kr.
*E-mail: ch45@zips.uakron.edu.

Notes

The authors declare no competing financial interest.

ACKNOWLEDGMENTS

This work has been supported by BRL (2015042417), MOTIE-KDRC (10051334) and BK21 Plus programs of Korea.

REFERENCES

(1) Steed, J. W.; Atwood, J. L. *Encyclopedia of Supramolecular Chemistry*; Marcel Dekker: Chichester, 2004.
(2) Reinhoudt, D. N. In *Supramolecular Materials and Technologies*; Isaacs, L., Chin, D. N., Bowden, N., Xia, Y., Whitesides, G. M.; John Wiley & Sons, Ltd.: New York, 1999; Chapter 1, pp 1−46.
(3) Hartgerink, J. D.; Beniash, E.; Stupp, S. I. Self-Assembly and Mineralization of Peptide-Amphiphile Nanofibers. *Science* **2001**, *294*, 1684−1688.
(4) Wang, Y.; Xu, H.; Zhang, Xi. Tuning the Amphiphilicity of Building Blocks: Controlled Self-Assembly and Disassembly for Functional supramolecular Materials. *Adv. Mater.* **2009**, *21*, 2849−2864.
(5) Yagai, S.; Nakajima, T.; Kishikawa, K.; Kohmoto, S.; Karatsu, T.; Kitamura, A. Hierarchical Organization of Photoresponsive Hydrogen-Bonded Rosettes. *J. Am. Chem. Soc.* **2005**, *127*, 11134−11139.
(6) Yan, X.; Wang, F.; Zheng, B.; Huang, F. Stimuli-responsive Supramolecular Polymeric Materials. *Chem. Soc. Rev.* **2012**, *41*, 6042−6065.
(7) Kobatake, S.; Takami, S.; Muto, H.; Ishikawa, T.; Irie, M. Rapid and Reversible Shape Changes of Molecular Crystals on Photoirradiation. *Nature* **2007**, *446*, 778−781.
(8) Abdallah, D. J.; Weiss, R. G. Organogels and Low Molecular Mass Organic Gelators. *Adv. Mater.* **2000**, *12*, 1237−1247.
(9) van Hameren, R.; Schön, P.; van Buul, A. M.; Hoogboom, J.; Lazarenko, S. V.; Gerritsen, J. W.; Engelkamp, H.; Christianen, P. C. M.; Heus, H. A.; Maan, J. C.; Rasing, T.; Speller, S.; Rowan, A. E.; Elemans, J. A. A. W.; Nolte, R. J. M. Macroscopic Hierarchical Surface Patterning of Porphyrin Trimers via Self-Assembly and Dewetting. *Science* **2006**, *314*, 1433−1436.
(10) Nath, N. K.; Pejov, L.; Nichols, S. M.; Hu, C.; Saleh, N.; Kahr, B.; Naumov, P. Model for Photoinduced Bending of Slender Molecular Crystals. *J. Am. Chem. Soc.* **2014**, *136*, 2757−2766.
(11) Yu, H.; Ikeda, T. Photocontrollable Liquid-Crystalline Actuators. *Adv. Mater.* **2011**, *23*, 2149−2180.
(12) Liu, Z.-X.; Feng, Y.; Yan, Z.-C.; He, Y.-M.; Liu, C.-Y.; Fan, Q.-H. Multistimuli Responsive Dendritic Organogels Based on Azobenzene-Containing Poly(ary ether) Dendron. *Chem. Mater.* **2012**, *24*, 3751−3757.
(13) Kreger, K.; Wolfer, P.; Audorff, H.; Kador, L.; Stingelin-Stutzmann, N.; Smith, P.; Schmidt, H.-W. Stable Holographic Gratings with Small-Molecular Trisazobenzene Derivatives. *J. Am. Chem. Soc.* **2010**, *132*, 509−516.
(14) Kim, D.-Y.; Lee, S.-A.; Kang, D.-G.; Park, M.; Choi, Y.-J.; Jeong, K.-U. Photoresponsive Carbohydrate-based Giant Surfactants: Automatic Vertical Alignment of Nematic Liquid Crystal for the Remote-Controllable Optical Device. *ACS Appl. Mater. Interfaces* **2015**, *7*, 6195−6204.
(15) Bushuyev, O. S.; Singleton, T. A.; Barrett, C. J. Fast, Reversible, and General Photomechanical Motion in Single Crystals of Various Azo Compounds Using Visible Light. *Adv. Mater.* **2013**, *25*, 1796−1800.
(16) Lee, J.; Oh, S.; Pyo, J.; Kim, J.-M.; Je, J. H. A light-driven Supramolecular Nanowire Actuator. *Nanoscale* **2015**, *7*, 6457−6461.
(17) Demus, D.; Goodby, J. W.; Gray, G. W.; Spiess, H.-W.; Vill, V. *Handbook of Liquid Crystals*; Wiley-VCH: New York, 1998.
(18) Kato, T.; Mizoshita, N.; Kishimoto, K. Functional Liquid-Crystalline Assemblies: Self-Organized Soft Materials. *Angew. Chem., Int. Ed.* **2006**, *45*, 38−68.
(19) Cantekin, S.; de Greef, T. F. A.; Palmans, T. F. A. Benzene-1,3,5-tricarboxamide: A Versatile Ordering Moiety for Supramolecular Chemistry. *Chem. Soc. Rev.* **2012**, *41*, 6125−6137.
(20) van Gorp, J. J.; Vekemans, J. A. J. M.; Meijer, E. W. C_3-symmetrical Supramolecular Architectures: Fibers and Organic Gels

DOI: 10.1021/acsami.6b03364
ACS Appl. Mater. Interfaces 2016, 8, 9490−9498

from Discotic Trisamides and Trisureas. *J. Am. Chem. Soc.* **2002**, *124*, 14759−14769.
(21) Lee, S.; Oh, S.; Lee, J.; Malpani, Y.; Jung, Y.-S.; Kang, B.; Lee, J. Y.; Ozasa, K.; Isoshima, T.; Lee, S. Y.; Hara, M.; Hashizume, D.; Kim, J.-M. Stimulus-Responsive Azobenzene Supramolecules: Fibers, Gels, and Hollow Sphers. *Langmuir* **2013**, *29*, 5869−5877.
(22) Kim, D.-Y.; Lee, S.-A.; Choi, Y.-J.; Hwang, S.-H.; Kuo, S.-W.; Nah, C.; Lee, M.-H.; Jeong, K.-U. Thermal- and Photo-Induced Phase-Transition Behaviors of a Tapered Dendritic Liquid Crystal with Photochromic Azobenzene Mesogens and a Bicyclic Chiral Center. *Chem. - Eur. J.* **2014**, *20*, 5689−5695.
(23) Kang, D.-G.; Kim, D.-Y.; Park, M.; Choi, Y.-J.; Im, P.; Lee, J.-H.; Kang, S.-W.; Jeong, K.-U. Hierarchical Striped Walls Constructed by the Photopolymerization of Discotic Reactive Building Blocks in the Anisotropic Liquid Crystal Solvents. *Macromolecules* **2015**, *48*, 898−907.
(24) Palmans, A. R. A.; Vekemans, J. A. J. M.; Fischer, H.; Hikmet, R. A.; Meijer, E. W. Extended-Core Discotic Liquid Crystals Based on the Intramolecular H-bonding in *N*-Acylated 2,2′-Bipyridine-3,3′-diamine Moieties. *Chem. - Eur. J.* **1997**, *3*, 300−307.
(25) Zhang, W.-B.; Yu, X.; Wang, C.-L.; Sun, H.-J.; Hsieh, I.-F.; Li, Y.; Dong, X.-H.; Yue, K.; Van Horn, R.; Cheng, S. Z. D. Molecular Nanoparticles Are Unique Elements for Macromolecular Science: From "Nanoatoms" to Giant molecules. *Macromolecules* **2014**, *47*, 1221−1239.
(26) Wu, K.; Huang, M.; Yue, K.; Liu, C.; Lin, Z.; Liu, H.; Zhang, W.; Hsu, C.-H.; Shi, A.-C.; Zhang, W.-B.; Cheng, S. Z. D. Asymmetric Giant "Bolaform-like" Surfactants: Precise Synthesis, Phase Diagram, and Crystallization-Induced Phase Separation. *Macromolecules* **2014**, *47*, 4622−4633.
(27) Hu, N.; Shao, R.; Shen, Y.; Chen, D.; Clark, N. A.; Walba, D. M. An Electric-Field-Responsive Discotic Liquid-Crystalline Hexa-peri-Hexabenzocoronene/ Oligothiophene Hybrid. *Adv. Mater.* **2014**, *26*, 2066−2071.
(28) Sun, H.-J.; Wang, C.-L.; Hsieh, I.-F.; Hsu, C.-H.; Van Horn, R. M.; Tsai, C.-C.; Jeong, K.-U.; Lotz, B.; Cheng, S. Z. D. Phase Behaviour and Janus Hierarchical Supramolecular Structures Based on Asymmetric Tapered Bisamide. *Soft Matter* **2012**, *8*, 4767−4779.
(29) Kim, D.-Y.; Wang, L.; Cao, Y.; Yu, X.; Cheng, S. Z. D.; Kuo, S.-W.; Song, D.-H.; Lee, S. H.; Lee, M.-H.; Jeong, K.-U. The biaxial lamella-columnar Liquid Crystalline Structure of a Tetrathiafulvalene Sanidic Molecule. *J. Mater. Chem.* **2012**, *22*, 16382−16389.
(30) Monshi, A.; Foroughi, M. R.; Monshi, M. R. Modified Scherrer Equation to Estimate More Accurately Nano-Crystallite Size Using XRD. *World J. Nano Sci. Eng.* **2012**, *2*, 154−160.
(31) Jeong, K.-U.; Jin, S.; Ge, J. J.; Knapp, B. S.; Graham, M. J.; Ruan, J.; Guo, M.; Xiong, H.; Harris, F. W.; Cheng, S. Z. D. Phase Structures and Self-assembled Helical Suprastructures via Hydrogen Bonding in a Series of Achiral 4-Biphenyl Carboxylic Acid Compounds. *Chem. Mater.* **2005**, *17*, 2852−2865.
(32) Jeong, K.-U.; Knapp, B. S.; Ge, J. J.; Graham, M. J.; Tu, Y.; Leng, S.; Xiong, H.; Harris, F. W.; Cheng, S. Z. D. Structures and Phase Transformations of Odd-Numbered Asymmetric Main-Chain Liquid Crystalline Polyesters. *Polymer* **2006**, *47*, 3351−3362.
(33) Pavia, D. L.; Lampman, G. M.; Kriz, G. S. In *Introduction to Spectroscopy*; Harcourt College Publishers: Austin, TX, 1996; Chapter 2, pp 14−82.
(34) Xue, C.; Jin, S.; Weng, X.; Ge, J. J.; Shen, Z.; Shen, H.; Graham, M. J.; Jeong, K.-U.; Huang, H.; Zhang, D.; Guo, M.; Harris, F. W.; Cheng, S. Z. D. Self-assembled "Supra-molecular" Structures via Hydrogen Bonding and Aromatic/Aliphatic Microphase Separation on Different Length Scales in Symmetric-Tapered Bisamides. *Chem. Mater.* **2004**, *16*, 1014−1025.
(35) Hwang, S.-H.; Park, S.-J.; Kim, H. Y.; Kuo, S.-W.; Lee, S. H.; Lee, M.-H.; Jeong, K.-U. Phase Behaviors and Structures of a Symmetrically Tapered Biphenylamide. *J. Phys. Chem. B* **2009**, *113*, 5843−5854.
(36) Choi, Y.-J.; Park, M.; Kim, D.-Y.; Hsu, C.-H.; Hwang, S.-H.; Jeong, K.-U. Butterfly-Shaped Diphenylpyrimidine Molecule: Tunable Photophysical Properties by Molecular Self-assembly Pathways. *J. Phys. Chem. Lett.* **2015**, *6*, 887−892.
(37) Miao, J.; Zhu, L. Hydrogen Bond-Assisted Supramolecular Self-Assembly of Doubly Discotic Supermolecules Based on Porphyrin and Triphenylene. *Chem. Mater.* **2010**, *22*, 197−206.
(38) Ryu, S. Y.; Kim, S.; Seo, J.; Kim, Y.-W.; Kwon, O.-H.; Jang, D.-J.; Park, S. Y. Strong Fluorescence Emission Induced by Supramolecular Assembly and Gelation: Luminescent Organogel from Nonemissive Oxadiazole-based Benezene-1,3,5-tricarboxamide Gelator. *Chem. Commun.* **2004**, *11*, 70−71.
(39) Bao, C.; Lu, R.; Jin, M.; Xue, P.; Tan, C.; Xu, T.; Liu, G.; Zhao, Y. Helical Stacking Tuned by Alkoxy Side Chain in π-Conjugated Triphenylbenzene Discotic Derivatives. *Chem. - Eur. J.* **2006**, *12*, 3287−3294.
(40) Chen, Q.; Feng, Y.; Zhang, D.; Zhang, G.; Fan, Q.; Sun, S.; Zhu, D. Light-Triggered Self-Assembly of a Spiropyran-Functionalized Dendron into Nano-/Micrometer-Sized Particles and Photoreponsive Organogel with Switchable Fluorescence. *Adv. Funct. Mater.* **2010**, *20*, 36−42.
(41) Tateishi, Y.; Tanaka, K.; Nagamura, T. Kinetics of Photoinduced *E* to *Z* Isomerization of Azobenzene in Polystyrene Films: Thickness, Molecular Weight and Temperature Effects. *J. Phys. Chem. B* **2007**, *111*, 7761−7766.
(42) Ma, N.; Wang, Y.; Wang, Z.; Zhang, X. Polymer Micelles as Building Blocks for the Incorporation of Azobenzene: Enhancing the Photochromic Properties in Layer-by-Layer Films. *Langmuir* **2006**, *22*, 3906−3909.
(43) Kim, D.-Y.; Lee, S.-A.; Park, M.; Choi, Y.-J.; Kang, S.-W.; Jeong, K.-U. Multi-responsible Chameleon Molecule with Chiral Naphthyl and Azobenzene Moieties. *Soft Matter* **2015**, *11*, 2924−2933.
(44) Shibaev, V.; Bobrovsky, A.; Boiko, N. Photoactive Liquid Crystalline Polymer Systems with Light-Controllable Structure and Optical Properties. *Prog. Polym. Sci.* **2003**, *28*, 729−836.
(45) Kim, D.-Y.; Lee, S.-A.; Choi, H. J.; Chien, L.-C.; Lee, M.-H.; Jeong, K.-U. Reversible Actuating and Writing Behaviours of a Head-to-Side Connected Main-Chain Photochromic Liquid Crystalline Polymer. *J. Mater. Chem. C* **2013**, *1*, 1375−1382.
(46) Yu, Y.; Nakano, M.; Ikeda, T. Directed Bending of a Polymer Film by Light. *Nature* **2003**, *425*, 145.
(47) Yu, Y.; Nakano, M.; Shishido, A.; Shiono, T.; Ikeda, T. Effect of Cross-linking Density on Photoinduced Bending Behavior of Oriented Liquid-Crystalline Network Films Containing Azobenzene. *Chem. Mater.* **2004**, *16*, 1637−1643.
(48) Ikeda, T.; Nakano, M.; Yu, Y.; Tsutsumi, O.; Kanazawa, A. Anisotropic Bending and Unbending Behavior of Azobenzene Liquid-Crystalline Gels by Light Exposure. *Adv. Mater.* **2003**, *15*, 201−205.
(49) Ikeda, T. Photomodulation of Liquid Crystal Orientations for Photonic Applications. *J. Mater. Chem.* **2003**, *13*, 2037−2057.

DOI: 10.1021/acsami.6b03364
ACS Appl. Mater. Interfaces 2016, 8, 9490−9498